Bioresource Technology Reports 35 (2026) 102947

Contents lists available at ScienceDirect

Bioresource Technology Reports

journal homepage: www.sciencedirect.com/journal/bioresource-technology-reports

Natural waxes from *Spartium junceum* L. stem residues: Effect of rehydration time on yield, composition, and antimicrobial properties

Chiara La Torre [a], Antonella Buccafuri [a], Maria Aponte [b], Anna di Blasio [b], Giuseppe Chidichimo [c], Paolino Caputo [c], Teresa Cerchiara [d], Alessia Fazio [a,*], Giuseppe Blaiotta [b]

[a] Department of Pharmacy, Health and Nutritional Sciences, University of Calabria, Via Savinio, 87036, Rende, CS, Italy
[b] Department of Agricultural Sciences, University of Naples "Federico II", Via Università 100, 80055, Portici, Na, Italy
[c] Department of Chemistry and Chemical Technologies, University of Calabria, Via Pietro Bucci, 87036 Arcavacata di Rende, CS, Italy
[d] Department of Pharmacy and Biotechnology, University of Bologna, Via San Donato 19/2, 40127, Bologna, Italy

ARTICLE INFO

Keywords:
Spartium junceum L.
Natural wax
LC-MS
SEM
DSC
Antimicrobial activity

ABSTRACT

Plant-derived waxes are attracting growing interest as renewable and sustainable alternatives to fossil-based materials, owing to their functional properties and broad applicability. Within this framework, the present study explored the valorisation potential of Spanish broom (*Spartium junceum* L.) stems through the recovery and chemical, thermal, and morphological characterization of waxes from their inner fibrous fraction. The effect of rehydration-assisted pre-treatment on wax extractability, chemical composition, supramolecular organization, and antimicrobial activity was systematically investigated. Broom stems were rehydrated for 2, 3, or 4 days prior to delamination and Soxhlet extraction with n-hexane. Wax recovery was strongly dependent on rehydration time, reaching a maximum after 3 days (≈2.3% w/w).

LC–MS/MS analysis revealed a conserved wax composition across all samples, dominated by long-chain fatty alcohols and wax esters forming homologous series extending to very-high-molecular-weight species (≥C56), consistent with plant cuticular wax biosynthesis. Despite similar qualitative profiles, significant differences in thermal and morphological properties were observed. Differential scanning calorimetry showed increasing melting temperatures and fusion enthalpies from 2D to 3D and 4D samples. These trends were confirmed by scanning electron microscopy, which evidenced a transition from weakly structured morphologies to organized crystalline networks a more homogeneous and continuous microstructures with increasing rehydration time.

Biological assays demonstrated selective antimicrobial activity against Gram-positive bacteria, particularly *Streptococcus pyogenes*, with waxes extracted after 3 and 4 days. The results highlight Spanish broom stems as a promising underexploited biomass for the production of functional natural waxes.

1. Introduction

In recent years, scientific and industrial interest in natural waxes has grown significantly in response to the need to develop renewable and environmentally friendly materials capable of replacing fossil-based or animal-derived compounds in a wide range of industrial applications. Owing to their natural origin and intrinsic functional properties, natural waxes represent a strategic class of materials within the framework of green chemistry and sustainable development (Sasounian et al., 2024). From a chemical perspective, natural waxes consist of complex mixtures dominated by very-long-chain aliphatic compounds, including n-alkanes, free fatty acids, fatty alcohols, wax esters, aldehydes, ketones, and sterols. These components confer pronounced water-repellent properties and protective barrier functions, reflecting the natural roles of waxes in plant and animal systems (Kończak et al., 2026).

Plant-derived waxes such as carnauba, candelilla, and rice bran wax have been extensively investigated for their ability to improve moisture resistance, surface properties, and to act as structuring or barrier agents

* Corresponding author.
E-mail address: a.fazio@unical.it (A. Fazio).

https://doi.org/10.1016/j.biteb.2026.102947
Received 10 February 2026; Received in revised form 16 July 2026; Accepted 20 July 2026
Available online 25 July 2026

in coatings and films (Pashova, 2023; Doan et al., 2017). The incorporation of natural waxes into starch- and gelatin-based edible films has resulted in a significant increase in hydrophobicity and water vapor barrier performance, highlighting the potential of these biobased materials for food packaging applications (Cheng et al., 2022).

In plants, waxes play a fundamental biological role by forming protective barriers against environmental stressors. Cuticular and epicuticular wax layers reduce non-stomatal water loss, limit damage caused by excessive solar and ultraviolet radiation, and contribute to plant defence against pathogens and herbivores (Rahman et al., 2021; Da Silva Andrade et al., 2018). Despite the extensive industrial use of plant waxes, detailed information on their molecular composition remains limited for many botanical sources. Furthermore, extraction procedures are known to significantly affect wax yield, composition, and functional properties, underlining the need for comprehensive chemical characterization to support industrial applications (Nghiem et al., 2018; Luo et al., 2024).

Commercial plant waxes are typically obtained from specific plant organs, such as seeds (e.g., soybean, sunflower, and rice bran waxes), fruits and berries, and leaves (e.g., carnauba wax from *Copernicia prunifera*), while others, such as candelilla wax, are extracted from the aerial parts of shrubs like *Euphorbia antisyphilitica* (Regert, 2009). Beyond traditionally exploited waxes (e.g., carnauba, candelilla, and rice bran wax), recent studies have explored new plant matrices and agricultural by-products as alternative sources of natural waxes. For instance, wax extraction from *Musa acuminata* (banana) biomass using organic solvents has been investigated, showing solvent-dependent yields and revealing the presence of hydrophobic components comparable to conventional natural waxes, which may be valorized for sustainable industrial applications (Singh et al., 2024).

Similarly, plant materials commonly regarded as waste or residues, such as pine needles, have been investigated for wax recovery and subsequent use in sustainable coatings exhibiting hydrophobic properties suitable for biodegradable surface treatments. These emerging sources fall within the broader category of lignocellulosic biomass, defined as plant materials primarily composed of cellulose, hemicellulose, and lignin, and widely available in agricultural and forestry residues such as cereal straw, sugarcane and sugarcane bagasse, grasses, wood residues, and forest by-products. Lignocellulosic biomass represents one of the most abundant renewable and non-food resources on Earth and constitutes a key feedstock for biorefinery processes and the development of bioproducts, including high-value materials beyond biofuels (e.g., bioethanol, bioplastics, and functional chemicals) (Gundupalli et al., 2021).

In this context, sugarcane bagasse, the fibrous residue from sugar production, has been extensively studied due to its high cellulose, hemicellulose, and lignin content, as well as for the extraction of value-added products such as waxes, aromatic compounds, and biobased materials. Valorization strategies often involve the integration of pretreatment and fermentation processes aimed at the sustainable production of biofuels and co-products (Ntunka et al., 2025). Recent reviews further emphasize that lignocellulosic biomass derived from agricultural residues (e.g., rice straw, wheat straw, corn stover), grasses, and forest residues represents an extremely broad feedstock for the production of advanced biofuels, biobased materials, and functional chemicals, owing to its abundance, sustainability, and conversion potential in integrated biorefinery processes (Rodionova et al., 2021).

Although the wax fraction in lignocellulosic biomass is relatively small, its removal through solvent-based dewaxing processes can improve sugar accessibility during bioconversion while simultaneously providing a wax fraction enriched in long-chain esters, alkanes, and fatty alcohols suitable for various industrial applications, including biorefinery platforms (Gundupalli et al., 2021). Within this framework, *Spartium junceum* L. (Spanish broom), known in Italy as ginestra, represents a promising yet underexplored plant resource. This Mediterranean shrub has attracted increasing interest as a natural, sustainable, and renewable source of fibers for textile and technical applications. Fiber extraction is performed using an innovative and environmentally friendly process known as (Chidichimo et al., 2023), which involves controlled rehydration of dried stems followed by mechanical separation. While this process enables efficient fiber recovery, it also generates significant amounts of residual biomass rich in non-structural components, including waxes.

The valorization of such processing residues aligns with circular economy and biorefinery principles, enabling the recovery of high-value compounds from agricultural or forestry by-products (Cherubini et al., 2009). However, despite the growing interest in *Spartium junceum* L. fibers, the wax fraction derived from broom stem residues has not yet been comprehensively investigated. To the best of our knowledge, detailed molecular characterization of *Spartium junceum* L. waxes, particularly regarding chain-length distribution and wax ester composition, has not been reported. Moreover, their potential biological activities, such as antimicrobial and antioxidant effects, remain largely unexplored.

In the framework of biomass valorization and circular economy, the processing of broom stems (*Spartium junceum* L.) routinely involves a delamination step to remove the outer cortex for fiber isolation. This process leaves behind an abundant, cellulose- and pectin-rich inner core tissue that is traditionally discarded as processing waste (Malyzhenkov et al., 2025). Rather than focusing on primary surface cuticular extracts, which are structurally limited in yield and challenging to isolate cleanly on an industrial scale, this study investigates a cascade biorefinery approach to valorize these inner core stem residues obtained through the Deshydrex process.

Specifically, we evaluate how dynamic aqueous rehydration pretreatments, conducted for 2, 3, or 4 days, affect the structural reorganization, composition, and process-driven redistribution of lipophilic fractions into these inner core tissues, in order to identify the treatment yielding the highest wax recovery. To achieve this, comprehensive chemical, morphological, and thermal characterizations were performed using LC–MS/MS, scanning electron microscopy (SEM), and differential scanning calorimetry (DSC), respectively. In addition, the antimicrobial activity of the extracted waxes was evaluated against Gram-negative and Gram-positive bacteria, as well as fungi, to assess the potential of these process-redistributed cuticular waxes as natural and sustainable functional ingredients.

2. Materials and methods

2.1. Materials

All the solvents were provided by Carlo Erba (Milan, Italy). Microorganisms were purchased from collections DSMZ (Deutsche Sammlung von Mikroorganismen und Zellkulturen GmbH, Braunschweig, DE) and ATCC (American Type Culture Collection ATCC, Manassas, VA, USA). Culture media, Tryptone Soy Broth (TSB) and Tryptone Soy Agar (TSA), were purchased from (OxoidTM, Thermo Fisher Scientific Inc., Waltham, MA, USA).

2.2. Sample preparation

Broom stems were collected from wild populations in San Fili, Cosenza (Calabria, Italy; coordinates: 39°20′20″ N, 16°08′39″ E) between April and May 2024 and subsequently air-dried under direct sunlight for 48 h to allow natural moisture loss. Following the drying phase, the stems were subjected to controlled rehydration for periods of 2, 3, and 4 days (hereafter referred to as 2D, 3D, and 4D). This rehydration step was achieved by maintaining a constant water flow rate of 5 L/min over the material with the water temperature strictly maintained at a controlled room temperature of.

25 ± 1 °C to ensure experimental reproducibility and prevent thermal degradation of surface components. After rehydration, the stems

were manually delaminated to remove the outer fibrous layers, thereby isolating the cellulose- and pectin-rich inner tissues (Malyzhenkov et al., 2025). From each batch, an identical aliquot (2 g) was collected for subsequent analytical procedures for wax extraction.

2.3. Wax extraction

Following the respective rehydration periods (2, 3, or 4 days), the outer cortex of the broom stems was manually removed, and the remaining inner core tissues were isolated, dried, and finely powdered. The powdered inner core biomass (2 g) was then subjected to wax extraction using a Soxhlet apparatus with 100 mL of n-hexane as the extraction solvent. The extraction process was carried out overnight using an external oil heating bath maintained at 80 °C to ensure exhaustive solubilization of the wax fraction (Silva et al., 2022; Simões et al., 2022). The resulting n-hexane extract was subsequently concentrated under reduced pressure using a rotary evaporator with the water bath maintained at a controlled temperature of 40 °C and a vacuum pressure of approximately 251 mmHg until a viscous wax-rich residue was obtained. This concentrate was then crystallized in absolute ethanol to promote the selective isolation of the wax components. Finally, the crystallized waxes were dried under vacuum in a vacuum desiccator at 40 °C and 0.01 mmHg for 5 h to remove residual solvent and to obtain a purified, stable wax fraction. To ensure the complete removal of any residual solvent, the mass of the purified wax fraction was monitored until a constant weight was achieved (with deviations <0.1 mg between consecutive weightings). Waxes extracted from stems after 2, 3, and 4 days of rehydration are denoted as 2D, 3D, and 4D, respectively, reflecting the structural and compositional redistribution achieved across the distinct treatment intervals.

2.4. Characterization of waxes using liquid chromatography–tandem mass spectrometry (LC-MS/MS)

HPLC analyses were performed using an Agilent Technologies 1200 series liquid chromatography system equipped with a G1379B degasser, a G1312A binary pump, and a G1329A autosampler. Prior to analysis, the purified wax fractions (2D, 3D, and 4D) were dissolved in methanol to achieve a final sample concentration of 1.5 μg/mL. Chromatographic separation was achieved by injecting a volume of 10 μL of the prepared wax solution into a ZORBAX Eclipse XDB-C18 column (3 μm particle size; 250 mm length; 4.6 mm internal diameter; Agilent Technologies, Santa Clara, CA, USA). The column temperature was strictly maintained at a controlled temperature of 40 °C to prevent any analyte precipitation during the run. The mobile phase consisted of 100% acetonitrile as Phase A (weak eluent) and 100% isopropanol as Phase B (strong eluent). A non-aqueous reversed-phase (NARP) gradient elution was executed at a constant flow rate of 350 μL/min. The optimized elution profile, spanning a total run time of 50 min to ensure full matrix resolution and column re-equilibration, was programmed as follows: 0–5 min, isocratic hold at 10% B (90% A); 5–25 min, linear gradient from 10% to 70% B (30% A); 25–40 min, linear gradient from 70% to 100% B (0% A) to elute the long-chain wax esters; 40–45 min, isocratic wash at 100% B; and 45–50 min, rapid return and final re-equilibration at 10% B (90% A). The mass spectrometer utilized for MS/MS analyses was an API 4000 Q-Trap (Applied Biosystem/MSD Sciex, Foster City, CA, USA). Mass spectrometry detection was performed using an electrospray ionization source operating in positive ion mode (ESI^+). To achieve structural characterization, the wax extracts were analyzed in Product Ion mode (MS2). The MS parameters, including the input potential (10.0 EP), declustering potential (70 DP), collision energy (35 CE), and collision exit potential (10 CXP) were optimized for the chosen transition. Acquisition took place between 50 and 1000 *m/z* with a scan time of 1 s per spectrum (Benincasa et al., 2021; Vrkoslav et al., 2013).

2.5. Differential scanning calorimetry (DSC)

The sample waxes were weighed precisely (~10 mg) and transferred into the DSC aluminum smelting bowl. It was capped and packed by moulding machine and the bowl was set into DSC apparatus (SETARAM 131 evo, LabWrench, Midland, ON, Canada). Cooling of the sample was done using liquid nitrogen, and then the sample was heated from 0 °C to 100 °C at the velocity of 10 °C/min. For the adequate melting of wax and the balance of instrumental baseline the maintaining time was 2 min. Then, the cooling of sample from 100 °C to 0 °C at the velocity of 10 °C/min by liquid nitrogen was also done. Both the heating and cooling scans were performed under a continuous purge of nitrogen gas as the shielding atmosphere (Bucio et al., 2021; Ruguo et al., 2011). The peak positions (°C) and enthalpy values (J/g) were determined by numerically integrating the area under each individual thermal peak relative to a linear baseline using the SETARAM software "SetSoft2000".

For complex or overlapping thermal events, peaks were resolved to ensure accurate and independent enthalpy attribution.

2.6. Scanning electron microscopy (SEM)

The morphological characterization of the samples was carried out using a Phenom ProX scanning electron microscope (SEM, Thermo Fisher Scientific Inc., Hillsboro, OR, USA) (La Torre et al., 2024; La Torre et al., 2021). A representative portion of each sample was mounted onto a standard 12 mm diameter SEM stub using double-sided adhesive tape. Loose particulate residues on both the sample surface and the support were removed by gentle air blowing prior to sputtering/metallization. Samples were covered with an ultrathin Au layer (10 nm) before investigation by using an Auto Sputter Coater (Agar, Cambridge, UK). Surface topography and compositional contrast were examined using secondary electron (SE) and backscattered electron (BSE) imaging modes, respectively. All SEM analyses were performed at an accelerating voltage of 5 kV. It is worth noting that a Peltier cooling stage was not utilized during the analysis. Micrographs were acquired at magnifications of 100×, 250×, and 500× to enable a comprehensive assessment of surface morphology and microstructural features.

2.7. Antimicrobial activity

The antimicrobial activity of wax extracts 2D, 3D, and 4D was assessed by the agar well diffusion assay (WDA), following the procedure described by Rossello et al. (2024) (Rossello et al., 2024). Gram-positive strains used as indicators were *Streptococcus* (*St.*) *pyogenes* ATCC 12344, *Staphylococcus* (*Staph.*) *aureus* DSM 799, and *Enterococcus* (*Ent.*) *hirae* ATCC 10541. Gram-negative strains were *Escherichia* (*E.*) *coli* NCTC 10538, *E. coli* ATCC 10536, and *Pseudomonas* (*P.*) *aeruginosa* ATCC 15442. *Candida* (C.) *albicans* ATCC 10231 and *Aspergillus* (*A.*) *brasiliensis* ATCC 16404 served as yeast and mould representatives (Table 3).

Serial two-fold dilutions of wax extracts in sterile DMSO were prepared. Specifically, the concentration range was 0.317–10.15, 0.353–11.30, and 0.375–6.00 mg/mL for wax extracts 2D, 3D, and 4D, respectively. For the antibacterial activity evaluation, 50 μL of each dilution was spotted into aseptically bored wells (6 mm in diameter) on Tryptone Soy Agar (TSA, Oxoid) previously seeded with about 106 CFU/mL of the target strain. To evaluate the antifungal activity, 0.1 mL of yeast cells (*C. albicans*) or fungal spores (*A. brasiliensis*) suspensions (approximately 105 CFU/mL) were spread onto Malt Extract Agar (MEA, Oxoid) plates. Wax dilutions (15 mL each) were spotted on the agar surface in coded points. Plates were incubated at 28 °C for 2 or 4 days, for yeast and moulds, respectively. Clear inhibitory zones in the coded points indicated an antifungal effect. Pure dimethyl sulfoxide (DMSO) was utilized as a negative control in all antimicrobial assays to verify that the solvent itself did not exert any inhibitory effect. No zones of inhibition or microbial growth restrictions were observed for DMSO, confirming that the recorded antimicrobial activity is entirely

attributable to the bioactivity of the broom-stem wax extracts.

Based on agar well diffusion assay results, the time-kill assay was only carried out for wax extracts 3D and 4D and exclusively against strains ATCC 12344 (*St. pyogenes*) and DSM 799 (*Staph. aureus*). In detail, strain suspensions (about 106 CFU/mL) in Tryptone Soy Broth (TSB, Oxoid) were added with wax extracts (1.0, 0.5, and 0.25 mg/mL) and analyzed by standard bacterial counting procedure on TSA at time 0, as well as after 24 and 48 h of incubation at 37 °C under semi-anaerobic (static) conditions. All tests were done in triplicate.

2.8. Statistical analysis

All experiments were performed in triplicate, and the resulting averages were subjected to statistical analysis. Differences in wax recovery, thermal transitions, and relative enthalpies from DSC data were analyzed using GraphPad Prism software (version 10.3.1, GraphPad Software, San Diego, CA, USA). Antimicrobial activity data were processed using XLStat software (version 2012.6.02, Addinsoft Corp., Paris, France). For all analyses, a two-way ANOVA was applied, followed by Tukey post-hoc test for multiple comparisons. In figures and tables, statistically distinct groups are designated by different lowercase and uppercase letters ($p < 0.05$). Where specific highly significant differences are highlighted within the main text, they are indicated by asterisks according to standard significance thresholds ($p < 0.05$ (*), $p < 0.01$(**), $p < 0.001$ (***), and $p < 0.0001$ (****)).

3. Results

3.1. Wax recovery

Powdered broom stems previously rehydrated for 2, 3, or 4 days yielded significantly different wax amounts (****$p < 0.0001$) following Soxhlet extraction with *n*-hexane: 14.1 ± 0.1 mg g^{-1} (≈ 1.41% w/w) for 2D, 22.9 ± 1.3 mg g^{-1} (≈ 2.29% w/w) for 3D, and 4.7 ± 0.2 mg g^{-1} (≈ 0.47% w/w) for 4D (Fig. 1).

The maximum wax yield observed for the 3D treatment (≈ 2.3%) indicates that a moderate rehydration period significantly enhances the recoverable wax content of the inner fiber fraction of broom stems. This effect is plausibly associated with improved removal of outer fibers and increased solvent accessibility to wax-containing tissues.

Several studies on wax extraction from lignocellulosic agricultural residues have reported substantially lower yields than those obtained from 3D-treated broom stems. Gundupalli et al. reported wax yields of 0.57%, 0.61%, and 1.69% from rice straw (RS), Napier grass (NG), and sugarcane bagasse (SB), respectively, using solvent extraction methods

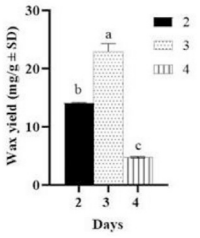

Fig. 1. Effect of rehydration time on the extraction yield of Spanish broom-stem waxes. Wax yields are expressed as weight percentage of dry biomass weight (% w/w) obtained across three different rehydration intervals: 2 days (2D, black column), 3 days (3D, dotted column), and 4 days (4D, striped column). Data are presented as mean values ± standard deviation (SD) of triplicate experiments ($n = 3$) that is indicated by bars on the histograms. Statistical analysis was performed via two-way ANOVA followed by Tukey post-hoc test for multiple comparisons using GraphPad Prism software (version 10.3.1). Lowercase letters above the bars indicate statistically distinct groups; different letters denote significant differences ($p < 0.05$), highlighting the time-dependent, non-linear trend of matrix disruption.

comparable in severity (Gundupalli et al., 2021). Similarly, Qi et al. recovered approximately 1.2% (w/w) crude wax from sugarcane bagasse using a petroleum ether/ethanol solvent system (Qi et al., 2017). Nghiem et al. reported wax yields ranging from 0.29% to 0.80% when extracting dried sorghum using boiling absolute ethanol (Nghiem et al., 2018).

Guo et al. reported higher values for primarily aliphatic and wax-like compounds obtained via single-step ethanol extraction from agricultural residues, with yields of 4.28% for corncob (CC), 6.57% for wheat straw (WS), and 1.41% for poplar sawdust (PS) (Guo et al., 2021). However, these values represent the total ethanol-soluble fraction rather than a selectively isolated wax fraction and thus are not directly comparable to *n*-hexane–extracted wax yields.

In this context, the ≈ 2.3% wax yield obtained from 3D-treated broom stems is comparatively high for a woody, lignocellulosic biomass under selective solvent-extraction conditions. This suggests that rehydrated and delaminated broom-stem inner fibers may represent a more promising source of extractable wax than many conventional agricultural residues.

It should be noted that higher wax yields have been reported for biomass rich in cuticular waxes, such as leaves and other non-structural tissues. For instance, Singh et al. investigated Soxhlet extraction of natural wax from *Musa acuminata* (banana) biomass using solvents of differing polarity, demonstrating that non-polar solvents such as hexane and toluene were most effective for wax recovery. They reported wax yields of 0.2–0.6 g from 10 to 15 g of banana leaves and 0.2–0.5 g from 20 to 25 g of banana peels (Singh et al., 2024).

However, banana biomass consists predominantly of non-woody, cuticle-rich tissues (leaves, peels, pseudostems), which differ fundamentally from the highly lignified inner fibers of broom stems. Consequently, such comparisons are only partially relevant. In this regard, the wax yield obtained from Spanish broom stems is particularly noteworthy, as it is achieved from a woody, highly fibrous biomass, underscoring the exceptional extractive potential of broom compared with softer, non-woody plant tissues.

Several factors may account for the comparatively high wax yield observed for broom stems subjected to the 3D treatment:

- Pre-treatment by rehydration and delamination
  Rehydration likely softened the structural matrix of the stem, facilitating mechanical separation and enhancing solvent access to wax-containing domains. Delamination removed outer fiber layers that may otherwise hinder solvent penetration, exposing more accessible inner tissues.
- Nature of broom-stem inner fibers
  Unlike many agricultural residues (e.g., straw or bagasse), where waxes are predominantly superficial and cuticular, broom stems may contain internal aliphatic or lipidic deposits, such as resins, subcuticular lipids, or bound waxes, that become extractable only after structural disruption. This high lipid concentration is closely linked to the plant ecological niche; the biomass was harvested from wild populations growing along roadside embankments. These environments expose the plants to intense abiotic stressors, such as high solar radiation, wind, and thermal stress from the pavement. As a xerophytic Mediterranean shrub, *S. junceum* has evolved to synthesize a robust wax system to prevent desiccation and UV damage (Gimeno et al., 2012). While in annual crops (like rice or sugarcane) waxes are often lost during processing, the waxes in Spanish broom are deeply protected within the longitudinal grooves of its perennial, photosynthetic stems, acting as a more concentrated and preserved reservoir of lipids.
- Selective isolation of the fiber fraction: By removing outer tissues and focusing on inner fibers, the extraction targets a more homogeneous material, reducing dilution by non-wax structural components and thereby increasing the apparent wax yield when expressed on a mass-of-fiber basis.

The relatively high wax yield obtained from broom-stem fibers suggests that this biomass, often regarded as agricultural or forestry waste, could be valorised as a novel source of natural wax. Given the established industrial interest in plant-derived waxes for applications including surface coatings, polishes, bioplastics, and bio-based composites, broom-stem wax may represent:

i) A renewable and low-cost feedstock for wax-based products, particularly in regions where broom plants are abundant;
ii) A sustainable alternative to fossil-derived waxes or conventional natural waxes obtained from non-woody tissues, thereby expanding the range of viable raw materials;
iii) A component of integrated biorefinery schemes, where multiple fractions (e.g., cellulose, hemicellulose, pectin, and wax) are recovered from a single biomass stream, increasing overall resource efficiency and economic value.

3.2. LC–MS/MS characterization of wax components

Wax extracts (1.5 ppm in methanol) referred as 2D, 3D, and 4D were analyzed using a QTRAP LC–MS/MS system operating in positive electrospray ionization mode. Data acquisition was performed in Product Ion (MS^2) mode, allowing structural characterization of wax-related compounds through collision-induced dissociation. Representative MCA scans are shown in Fig. 2.

Across all samples, a series of high-*m/z* precursor ions (which represent the intact, unfragmented molecules tagged with a positive charge) ranging from m/z 409.6 to 871.7 was detected and assigned to long-chain wax-related compounds. Identification was achieved through comparison of m/z values, retention behavior, and MS/MS fragmentation patterns with those reported for authentic wax ester standards in the literature (Table 1). In ESI^+–MS/MS, wax esters form stable protonated molecules $[M+H]^+$. When these molecules are fragmented into the mass spectrometer, they undergo specific breakages known as diagnostic neutral losses, meaning they shed predictable, uncharged molecular pieces corresponding to their constituent fatty alcohol (R'OH) or fatty acid (RCOOH) units. Because these losses act as structural fingerprints, tracking them allows researchers to easily identify the building blocks of esterified lipids.

As detailed in Table 1, mono-oxygenated compounds detected at m/z 409.6 and 437.6 exhibited limited fragmentation, with dominant neutral losses of 18 Da (H_2O) and 32 Da (CH_3OH), consistent with long-chain fatty alcohols commonly present in plant waxes. These components contribute to the hydrophobic barrier properties of the wax layers (Xue et al., 2017).

Di-oxygenated species (O_2), spanning from C30 to C60, showed diagnostic neutral losses of 256–298 Da, corresponding to C16–C18 fatty acid or alcohol units. These losses are characteristic of ester bond cleavage and confirm the assignment of these compounds as wax esters composed of long-chain saturated moieties. The repeated observation of these neutral losses across homologous series differing by 14 Da (the mass of a repeating -CH2 methylene unit) further confirms the presence of linear aliphatic structures typical of plant-derived waxes.

The compound detected at *m/z* 832.6 ($C_{56}H_{114}O_3$) showed combined losses of fatty chain units and small neutral molecules, suggesting additional oxygenated functionality, such as hydroxylation or oxidation. Similar oxidized wax esters have been reported in plant cuticular waxes and agro- industrial residues. A schematic overview of these identified chemical structures and their corresponding fragmentation pathways is provided in Fig. 3.

As comprehensively detailed in Table 1, the results highlight major compositional shifts rather than minor qualitative fluctuations across the treatment days:

- Ester Fingerprint Simplification: the 2D wax profile is highly heterogeneous, featuring significant high-molecular-weight esters (e.g., *m/z* 615.5, 649.6, and 759.6 exhibiting High to Medium abundances between 24% and 54%). Conversely, in the 3D and 4D stages, the matrix undergoes a sharp consolidation where the C36 wax ester (*m/z* 537.8) becomes the absolute dominant Base Peak (100%), while its isomer (m/z 553.8) scales up significantly to a high abundance of 88% in 4D.
- Hydrolysis and Degradation Trends: A at the 4D stage, we observe a substantial quantitative increase in the C28 free wax alcohol (*m/z* 409.6), which jumps from 12% (low) in 3D to 36% (high) in 4D, suggesting partial ester cleavage.
- Oxidative Marker Accumulation: Crucially, the hydroxylated/oxidized ester marker at m/z 832.6 exhibits a steady, clear upward accumulation trend across the treatment days, rising from 12% (2D) → 18% (3D) → 26% (4D). This quantitative shift strongly corroborates our thermal (DSC) and extraction yield data, proving a progressive structural oxidation when the process is extended to 4 days.

Despite these significant dynamics, the wax profiles obtained from 2D, 3D, and 4D samples showed a conserved core composition, with several wax esters consistently detected across all conditions e.g., the C28 wax alcohol at *m/z* 409.6 [$C_{28}H_{57}O$], the C30 ester at m/z 453.6 [$C_{30}H_{61}O_2$], the main C36 wax ester at m/z 537.8 [$C_{36}H_{70}O_2$], the C40 wax ester at m/z 611.6 [$C_{40}H_{78}O_2$], and the oxidized compound at m/z 832.6 [$C_{56}H_{114}O_3$]. This suggests that the primary wax constituents originate from the plant-based substrate and are largely preserved during processing.

On the other hand, higher-molecular-weight wax esters ($\geq C_{42}$) were predominantly detected in the 2D sample, while their occurrence in 3D and 4D was limited or absent. This behavior may reflect differences in matrix complexity, extraction efficiency, or ionization performance rather than complete removal of these compounds. Similar trends have been reported for long-chain wax esters analyzed by LC– MS/MS, where detectability decreases with increasing chain length (Lísa and Holčapek, 2015).

The chain-length distributions observed in our LC–MS/MS analysis are consistent with patterns reported for plant cuticular waxes, which are complex mixtures of very-long-chain aliphatics and their derivatives. Cuticular waxes are typically composed of very-long-chain fatty acids (VLCFAs; generally C20–C34) and their downstream products such as alkanes, primary and secondary alcohols, aldehydes, ketones, and esters, forming homologous series with broad carbon ranges that reflect conserved biosynthetic pathways in plants (Wang et al., 2020). VLCFAs and their derivatives have been identified across diverse plant species, where the major aliphatic components frequently range between C20 and C40, and esterified lipids often extend to even higher carbon numbers depending on species and tissue type (Tunstad et al., 2024; Guo et al., 2021). Comparative studies of cuticular wax compositions have shown that homologous series are dominated by specific chain lengths such as C26–C32 for alcohols and fatty acids, while alkyl esters and other complex wax constituents may span from C36 up to ≥C56 depending on structural combinations of fatty acid and alcohol moieties (Hao et al., 2024). The presence of even-chain esters in our samples (e.g., C36, C40, C44) and very high-molecular-weight species (e.g., C56, C60) mirrors these literature trends and supports the conclusion that the wax profiles measured here reflect conserved very-long-chain aliphatic biosynthetic pathways in plant cuticles. Furthermore, the repeated observation of homologous series differing by 14 Da (–CH_2– units) aligns with typical patterns seen in linear aliphatic structures of plant waxes (Wang et al., 2020). The presence of long-chain wax esters and fatty

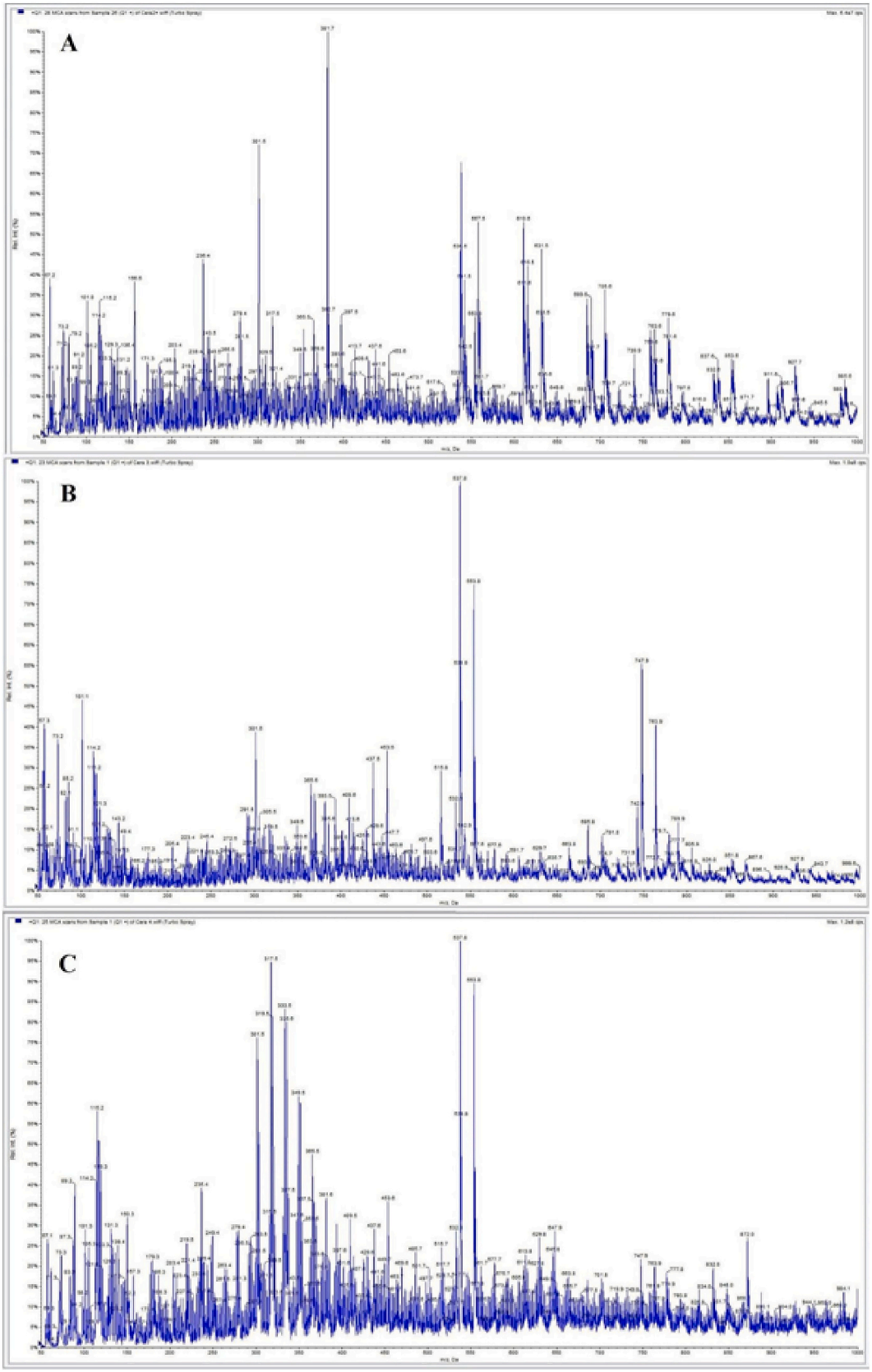

Fig. 2. Multiple channel acquisition (MCA) mass spectra of broom-stem wax extracts. The profiles were recorded in $Q1^+$ mode using a QTRAP LC–MS/MS system equipped with an electrospray ionization (ESI) source operating in positive ion mode. Spectra correspond to the wax fractions isolated after different rehydration times: (A) 2 days (2D), (B) 3 days (3D), and (C) 4 days (4D). The graphs illustrate the fingerprint distribution of high-*m/z* precursor ions spanning from m/z 409.6 to 871.7, corresponding to protonated molecular species $[M+1]^+$ of long-chain fatty alcohols, linear wax esters, and oxygenated derivatives. Variations in peak intensities and composition reflect differences in wax profiles among the three different rehydration times.

Table 1
Identification and structural assignment of broom-stem wax components across different rehydration intervals (2D, 3D, and 4D) via LC–MS/MS.[a]

Precursor ion (*m/z*)	Formula	Diagnostic neutral loss (Da)	Structural interpretation	2D	Int. (%)	3D	Int. (%)	4D	Int. (%)
409.6	$^{C}28^{H}57^{O}$	−18/−32	C28 wax alcohol; loss of H_2O/CH_3OH typical of long-chain alcohols	✓	22	✓	12	✓	36
437.6	$^{C}30^{H}61^{O}$	−18/−32	C30 wax alcohol	✓	16	✓	36	✓	28
453.6	$^{C}30^{H}61^{O}2$	−256	Ester: loss of C16H32O₂(palmitate)	✓	19	✓	38	✓	39
537.8	$^{C}36^{H}70^{O}2$	−256/−284	C36 ester: loss of C16 or C18	✓	52	✓	100	✓	100
553.8	$^{C}36^{H}70^{O}2$	−270/−284	C36 ester with different acid/alcohol combination	✓	29	✓	73	✓	88
561.7	$^{C}38^{H}72^{O}2$	−284	Ester containing C18 unit	✓	42	n. d.		✓	24
591.8	$^{C}40^{H}77^{O}2$	−284	C40 ester with possible unsaturation	✓	13	✓	11	n. d.	
611.6	$^{C}40^{H}78^{O}2$	−284/−298	C40 ester; C18–	✓	32	✓	23	✓	14
615.5	$^{C}42^{H}80^{O}2$	−298	C42 ester	✓		n. d.		n. d.	
649.6	$^{C}44^{H}86^{O}2$	−298	C44 ester	✓		n. d.		n. d.	
705.6	$^{C}48^{H}97^{O}2$	−256/−284	C48 ester; mixture of C18 units	✓		✓	17	n. d.	
732.9	$^{C}50^{H}101^{O}2$	−284	C50 ester	✓		✓	14	n. d.	
759.6	$^{C}52^{H}102^{O}2$	−284/−298	C52 ester	✓		n. d.		n. d.	
763.6	$^{C}53^{H}94^{O}2$	−298	C53 ester possible with CID rearrangement	✓		✓	14	n. d.	
816.0	$^{C}56^{H}114^{O}2$	−284/−298	High molecular weight C56 ester	✓		n. d.		n. d.	
832.6	$^{C}56\ ^{H}114^{O}3$	−284/+18	Oxidized/hydroxylated ester	✓	12	✓	18	✓	26
871.7	$^{C}60^{H}120^{O}2$	−298	C60 ester	✓	n.d.			✓	11

[a] Data were acquired using a QTRAP mass spectrometer operating in positive electrospray ionization mode (ESI^+). Precursor ions represent the protonated molecular species $[M + 1]^+$ detected in $Q1^+$ mode. Diagnostic neutral losses (expressed in Daltons, Da) indicate characteristic theoretical or literature-reported uncharged fragments used as molecular fingerprints for structural interpretation. Relative intensities (abbreviated as Int.) are expressed as percentages (%) normalized automatically by the software to the base peak (100%) of each specific Q1 MS profile. The absence of a constituent is indicated by "n.d." (not detected).

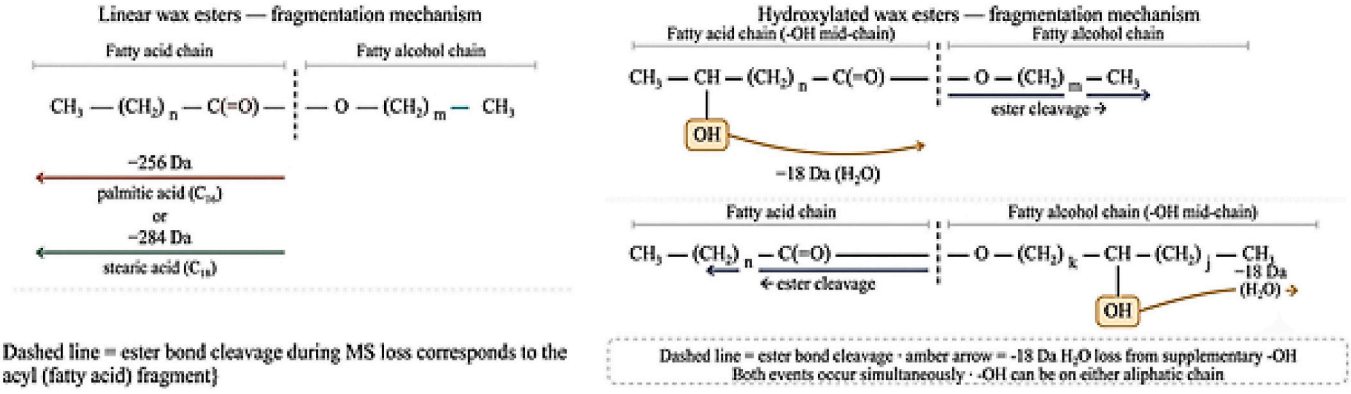

Fig. 3. Proposed MS/MS fragmentation mechanisms for linear (left) and hydroxylated (right) wax esters. The vertical dashed line indicates the primary ester bond cleavage site (C-O junction). Leftward arrows denote diagnostic neutral losses corresponding to the fatty acid acyl fragments (−256 Da for palmitic C16; −284 Da for stearic C18). Amber curved arrows represent the secondary, concurrent elimination of water (−18 Da, H2O) from mid-chain hydroxyl groups (-OH), occurring regardless of whether the modification is located on the acyl or alkyl moiety. Variables n, m, k, and j define the respective carbon chain lengths. (For interpretation of the references to color in this figure legend, the reader is referred to the web version of this article.)

alcohols highlights the potential of plant-derived residues as sources of valuable wax fractions. Such compounds are of interest for applications in cosmetics, coatings, lubricants, and bio-based materials.

The use of LC–MS/MS provides a robust analytical approach for wax characterization in complex substrates, supporting future efforts aimed at process optimization and resource valorization.

3.3. Differential scanning calorimetry (DSC) analysis

The thermal behavior of samples 2D, 3D, and 4D was investigated by DSC during heating and cooling cycles, as shown in Figs. 4 and 5, respectively. During the heating scan (Fig. 4), all samples exhibited endothermic transitions associated with melting processes. According to the literature, thermal events occurring between 40 °C and 60 °C in natural waxes and fatty systems are commonly attributed to the melting of free fatty acids and hydrocarbons. Conversely, transitions observed between 60 °C and 80 °C are mainly related to the fusion of fatty acid esters, which require higher energy due to their more stable molecular packing (Zhang et al., 2011). In agreement with this, the thermograms in Fig. 3 display distinct endothermic peaks corresponding to the melting of free fatty acids and hydrocarbons, which are labeled with the letter "a". A clear shift of these main endothermic peaks (peak "a") toward higher temperatures, accompanied by a significant increase in enthalpy, was observed when moving from sample 2D to samples 3D and 4D. In

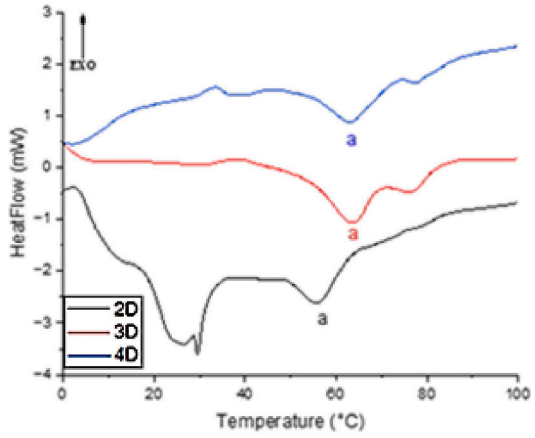

Fig. 4. DSC heating thermograms of the isolated broom-stem wax fractions. The curves illustrate the endothermic profiles and phase transition behaviors of the waxes extracted after 2 days (2D, black line), 3 days (3D, red line), and 4 days (4D, blue line) of rehydration. The endothermic peaks correspond to the melting pathways of the organized solid domains formed by the very-long-chain aliphatic components, where variations in peak shapes, onset temperatures (T), and melting enthalpies (ΔHm) reflect differences in the structural composition and purity of the extracted wax matrices. (For interpretation of the references to color in this figure legend, the reader is referred to the web version of this article.)

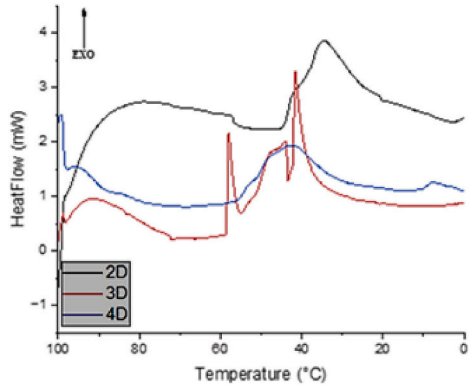

Fig. 5. DSC cooling thermograms of the isolated broom-stem wax fractions. The curves illustrate the exothermic profiles and solidification behaviors of the waxes extracted after 2 days (2D, black line), 3 days (3D, red line), and 4 days (4D, blue line) of rehydration. The exothermic peaks correspond to the structural alignment and solidification pathways of the very-long-chain aliphatic components upon cooling, where variations in peak shapes reflect differences in the molecular composition and packing dynamics of the extracted lipid matrices. (For interpretation of the references to color in this figure legend, the reader is referred to the web version of this article.)

particular, this thermal event shifted from 56.0 °C (ΔH = 5.04 J/g) in sample 2D to 63.3 °C (ΔH = 22.57 J/g) in sample 3D, and to 62.8 °C (ΔH = 27.22 J/g) in sample 4D (Table 2). This marked increase in both melting temperature and enthalpy strongly indicates an enhanced thermal stability and a higher degree of molecular organization in the modified samples (3D and 4D). Similar behavior has been widely reported for waxes and lipid-based materials, where higher thermal parameters are associated with stronger intermolecular interactions and a more homogeneous and continuous microstructures (Freitas et al., 2018; Irimia et al., 2025; Tavernier et al., 2017). Moreover, the presence of additional melting peaks in the higher temperature range for samples 3D (71.8 °C; ΔH = 3.67 J/g) and 4D (78.8 °C; ΔH = 1.26 J/g) indicated a larger contribution of esterified or highly ordered lipid fractions compared to sample 2D. This observation suggested that structural

Table 2
Thermodynamic parameters of the primary endothermic transition (peak a) for broom-stem wax fractions isolated after 2 days (2D), 3 days (3D), and 4 days (4D) of rehydration.[†]

Sample	Thermal transition (°C)			ΔH (enthalpy) (J/g)
	Low-temperature peak	Peak a	High-temperature peak	
2D		56.0 ± 2.0^{a,C}		5.04^{b,D}
2D	29.5 ± 0.6^{b,A}			18.58^{a,C}
3D		63.3 ± 3.4^{b,A}	71.8 ± 3.7^{a,B}	22.57^{a,B}
3D				3.67^{b,E}
4D		62.8 ± 2.9^{b,B}		27.22^{a,A}
4D			78.8 ± 2.9^{a,A}	1.26^{b,F}

Values represented the mean of independent experiments performed in triplicate ± the standard deviation. Letters indicate the significance of the data. Values with different letters are significantly different. Lower-case letters indicate statistically significant differences within the same sample. Uppercase letters indicate significant differences between different samples ($p < 0.05$) according to two-way ANOVA followed by Tukey post-hoc test.

[†] Thermal transition temperatures (°C) and enthalpies of fusion (ΔH, J/g dry wax) were determined via DSC heating thermograms. Peak a denotes the main thermal event associated with the melting of free fatty acids and hydrocarbons.

modifications occurring in samples 3D and 4D favored the formation of more energetically stable crystalline domains, likely associated with longer alkyl chains or improved chain alignment.

Interestingly, this high-temperature endothermic signal is more pronounced in the 3D sample and becomes less evident in the 4D sample. This behavior suggests that while a 3-day treatment maximizes the recovery and organization of the esterified fractions, further processing up to 4 days might lead to a relative reduction or structural dilution of these specific components, thereby decreasing the overall enthalpy of this transition.

On the other hand, an endothermic peak at 29.5 °C (ΔH = 18.58 J/g) was detected exclusively in sample 2D. This peak indicates specific phase transitions related to the crystalline structure or the melting of low-melting-point components (Principato et al., 2021). The complete absence of this transition in samples 3D and 4D is likely due to a significant reduction in the low-melting-point components of the initial material during the processing and rehydration steps.

The cooling thermograms (Fig. 5) exhibited a more complex pattern than the heating scans, with multiple exothermic peaks, particularly evident for sample 3D. This behavior was attributed to the higher sensitivity of crystallization processes to kinetic factors such as nucleation rate, molecular mobility, and cooling history. Unlike melting, which is primarily governed by thermodynamic equilibrium, crystallization is strongly influenced by kinetic constraints, often resulting in the formation of multiple crystalline populations (Padar et al., 2008; Guo et al., 2005; Righetti, 2017). The presence of multiple crystallization peaks suggested the coexistence of different polymorphic forms or fractions crystallizing at different temperatures, a phenomenon commonly observed in lipid-based and waxy materials.

The differences became even more pronounced when considering the enthalpy of fusion reported in Table 2. Sample 2D exhibited a significantly lower enthalpy of fusion (5.04 J/g) compared to samples 3D (22.57 J/g) and 4D (27.22 J/g), which showed comparable values. Since the enthalpy of fusion is directly related to the amount of crystalline phase present in a material, these results indicated a markedly lower degree of crystallinity in sample 2D.

Higher enthalpy values are generally associated with stronger intermolecular interactions and a higher degree of molecular packing efficiency, leading to more stable and ordered crystalline domains (Saher et al., 2024). In lipid- and wax-based systems, an increase in fusion enthalpy has been correlated with a higher content of long-chain

fatty acid esters and improved chain alignment (Brykczynski et al., 2025a; Liu et al., 2024). Therefore, the significantly higher enthalpy values observed for samples 3D and 4D suggested a more developed crystalline network compared to sample 2D.

Furthermore, the similar melting peak temperatures observed for samples 3D and 4D, combined with the higher enthalpy measured for sample 4D, indicated that while the crystal type and melting mechanism were comparable, sample 4D contained a larger fraction of crystalline domains and/or a higher degree of molecular organization. This difference may be attributed to variations in molecular arrangement or crystallite size distribution, which can significantly affect the overall enthalpy without substantially shifting the melting temperature.

Overall, the combined DSC results demonstrated that the transition from 2D to 3D and 4D samples led to:

(i) an increase in melting temperatures;
(ii) a substantial rise in fusion enthalpy;
(iii) more complex crystallization behavior during cooling.

These findings pointed to an evolution toward a more ordered and thermally stable structure, consistent with trends reported for bio-based waxes and lipid-derived materials used in industrial and agricultural applications, where enhanced crystallinity is often associated with improved mechanical and thermal performance.

3.4. SEM morphology analysis

The SEM micrographs (Fig. 6) highlighted marked differences in surface morphology and solid-state organization among samples 2D, 3D, and 4D, revealing a progressive evolution of the surface topography that correlated with the distinct thermal signatures observed by DSC. It is worth noting that due to the highly thermosensitive nature of these lipid-based materials under the electron beam, which precludes a reliable quantitative analysis of porosity or crystal size distribution, SEM was employed in this study primarily as a qualitative tool to observe macrostructural and surface evolution.

Sample 2D (first row) exhibited a relatively compact and continuous morphology. At low magnification, the surface appeared dense and homogeneous, while higher magnifications revealed a wavy and irregular topography with limited textural differentiation. At 500× magnification, the material largely behaved as a single consolidated block, with no clear evidence of discrete phase-separated domains. The observed roughness appeared to arise primarily from surface undulations rather than from distinct structural arrangements, suggesting a lower degree of supramolecular organization and a less heterogeneous solid network. Such compact and featureless morphologies have been reported in lipid and wax systems characterized by limited structural definition, where poorly developed networks correspond to reduced thermal transitions in DSC profiles (Pipintakos et al., 2022).

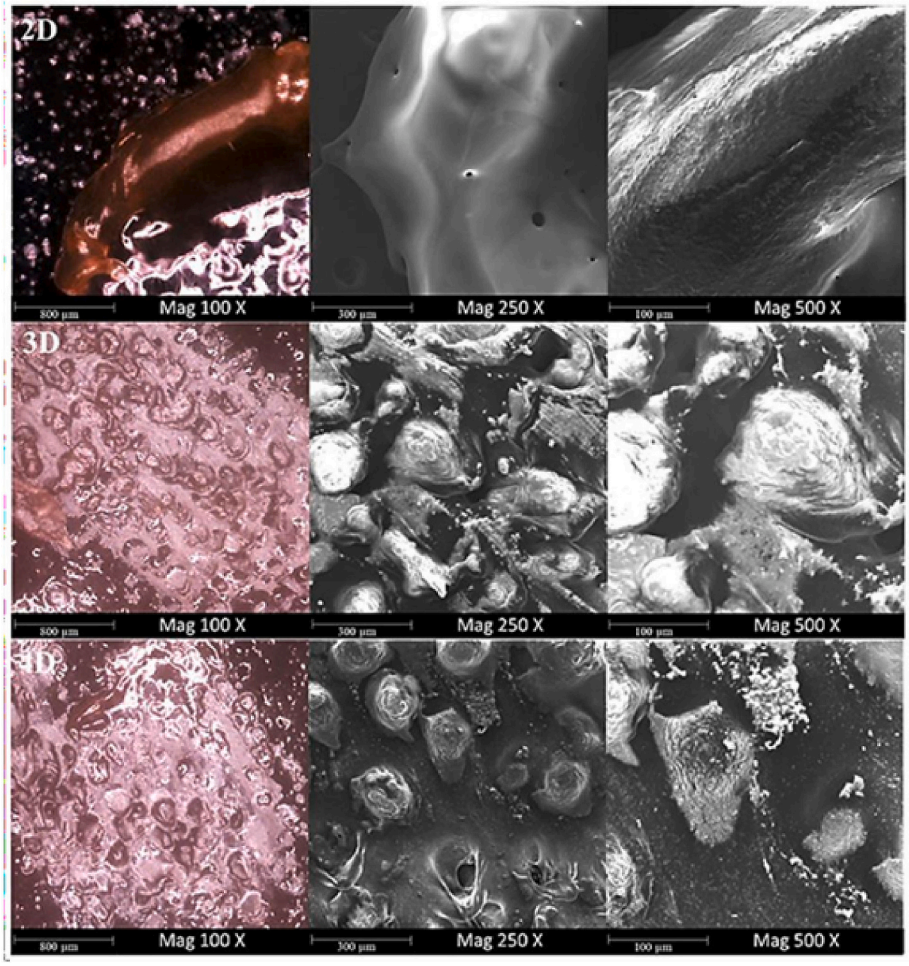

Fig. 6. SEM micrographs of Spanish broom-stem fibers showing morphological changes across different rehydration intervals. Representative surface views are presented for samples subjected to 2 days (2D), 3 days (3D), and 4 days (4D) of rehydration. Each sample series was analyzed at three progressive magnifications to capture different structural scales: 100× magnification (scale bar = 800.0 μm) providing an overview of fiber bundle macro-organization; 250× (scale bar = 300.0 μm) illustrating surface uniformity and delamination dynamics; and 500× (scale bar = 100.0 μm) revealing micro-structural details, surface roughness, and localized matrix disruption.

In contrast, sample 3D (second row) showed a substantially different morphology, displaying a more heterogeneous surface arrangement. The surface was characterized by well-defined macroscopic domains embedded within a rough matrix. These features appeared as rounded or platelet-like structures, clearly distinguishable from the surrounding phase. At higher magnifications, these macrostructures were covered by finer microtopographic features, indicating a multiscale morphological arrangement. Similar structures have been observed in triglyceride and lipid systems, where the development of multiple structural levels leads to complex surface morphologies and influences thermal behavior (Bayés-García et al., 2024). The morphological complexity of sample 3D corresponded to the higher fusion enthalpy recorded in the DSC heating scans, suggesting a larger fraction of ordered material and stronger intermolecular interactions. Furthermore, the coexistence of macro- and micro-features supported the presence of multiple molecular populations, consistent with the complex exothermic transitions observed during cooling.

Sample 4D (third row) further accentuated these morphological features, exhibiting a more homogeneous, dense, and continuous solid state compared to the baseline material. Although macroscopic domains were still evident, their distribution appeared more uniform, and the rough matrix was significantly more extended compared to sample 3D. High-magnification images revealed a denser population of micro-features decorating both the macrostructures and the surrounding matrix, indicating a higher density of nucleation events and the formation of a more interconnected framework. Such progression has also been reported in wax–oil mixtures and oleogel systems, where denser and more intricate frameworks form under controlled conditions, leading to higher fusion enthalpies and improved thermal stability (Brykczynski et al., 2025b). The increased surface roughness and multiscale organization observed for sample 4D correlated with the highest fusion enthalpy values measured, reflecting a more developed and stable solid framework with improved molecular packing efficiency. Overall, the SEM analysis revealed a clear morphological transition from a compact and weakly structured material in sample 2D to a dense and continuously rearranged solid system in samples 3D and 4D, with an increasing presence of distinct surface domains and roughness. This evolution reflected enhanced molecular ordering and structural efficiency in the modified samples, in close agreement with the thermal behavior observed by DSC and consistent with recent studies on lipid and wax-based materials where the development of the solid-state architecture directly influences both morphology and thermal properties (Rinaldi et al., 2015).

3.5. Antimicrobial activity

By the well diffusion assay, none of the wax extracts exhibited inhibitory activity against the tested Gram-negative strains (Table 3). The only strain of Gram-positive bacteria that was sensitive to extract 2D was *St. pyogenes* ATCC 12344. When the extracts 3D and 4D were tested against *St. pyogenes*, *Staph. aureus*, and *Ent. hirae*, no discernible changes in inhibition zone diameters could be noticed. Yeasts and moulds showed a higher tolerance to wax extracts. *C. albicans* was susceptible to all three extracts but only when tested at the highest concentrations, indicating a dose-dependent antifungal effect (Table 3).

Based on the results, 3D and 4D wax extracts were further evaluated by time–kill assay against *Staph. aureus* and *St. pyogenes* strains. Tests were carried out at three concentrations (1.0, 0.5, and 0.25 mg/mL) to distinguish between bactericidal and bacteriostatic effects. The two species displayed markedly different responses. Extract 3D induced about a one-log in *Staph. aureus* and the effect appeared to be dose-independent (Fig. 7, Panel A), suggesting a bacteriostatic activity. By contrast, the 4D extract showed a noticeable antimicrobial effect, but only when tested at the highest concentration (1.0 mg/mL): 3-log drop was observed during the early hours of exposure, whereas by 24 h, cell counts fell below the detection limit of the method (<1 log CFU/mL) (Fig. 7, Panel B). Such behavior testifies to a bactericidal effect.

The response of *St. pyogenes* to both wax extracts was substantially different and markedly stronger. Regardless of the extract used, concentrations of 1.0 and 0.5 mg/mL resulted in rapid population decline: counts dropped below the threshold limit already after 24 h (Fig. 7, Panels C and D). Even at the lowest tested concentration (0.25 mg/mL), both extracts exerted a noticeable effect, with extract 3D characterized by a stronger inhibitory effect. Notably, the 4D extract had an immediate effect against *St. Pyogenes*: the wax extract at 0.5 and 1.0 mg/mL concentrations induced a 3-log reduction already at time zero. A similar effect was detected for extract 3D, but only at the highest tested concentration. In this case, differences in bacterial counts at time 0 were statistically significant ($p < 0.05$) (Fig. 7, Panel C), suggesting a rapid and direct interaction between the wax constituents and the bacterial cell envelope.

4. Discussion

The results obtained in this study highlighted a strong interdependence between rehydration-assisted extraction conditions, chemical composition, supramolecular organization, and biological activity of waxes isolated from broom-stem inner fibers. Rather than acting independently, these factors evolved in a coordinated manner as a function of rehydration time, ultimately determining both the physicochemical properties and the antimicrobial performance of the extracts.

From a process perspective, the rehydration step played a pivotal role in modulating wax recovery and accessibility. The markedly higher wax yield obtained after 3 days of rehydration suggested that moderate hydration optimally disrupts the lignocellulosic matrix, facilitating delamination and solvent penetration without inducing excessive leaching or loss of extractable lipophilic components. Similar effects of biomass pre-treatment on extractive accessibility have been reported for agricultural residues and woody substrates, where controlled hydration enhances solvent diffusion and extractability of waxy fractions (Gundupalli et al., 2021; Qi et al., 2017). In contrast, prolonged rehydration (4D) appears to reduce the recoverable wax fraction indicating that wax availability depends not only on its intrinsic content but also on its physical confinement within the fiber network.

This sharp decline (****$p < 0.0001$) suggests that the benefits of rehydration are strictly time-dependent. During the experimental

Table 3
Antimicrobial activity of isolated broom-stem wax extracts against bacterial and fungal strains.

Wax extracts	Concentration range (mg/mL)	*Strep. pyogenes* ATCC12344	*Staph. aureus* DSM 799	*Ent. hirae* ATCC 10541	*E. coli* NCTC 10538	*E. coli* ATCC 10536	*P. aeruginosa* ATCC 15442	*C. albicans* ATCC 10231	*A. brasiliensis* ATCC 16404
2D	10.15–0.317	0.634[a]	-	-	-	-	-	10.15	-
3D	11.30–0.353	0.706	0.706	0.706	-	-	-	11.30	-
4D	6.00–0.375	0.750	0.750	0.750	-	-	-	6.00	6.00

The numerical values reported under each microbial strain represent the Minimum Inhibitory Concentrations (MIC), and their unit of measurement is mg/mL (corresponding to the specific active dilution tested). Inactive conditions or concentrations showing no inhibition are indicated by a hyphen (-).

[a] The lowest active dilution (mg/mL) that produced an inhibition halo measuring at least 1 mm.

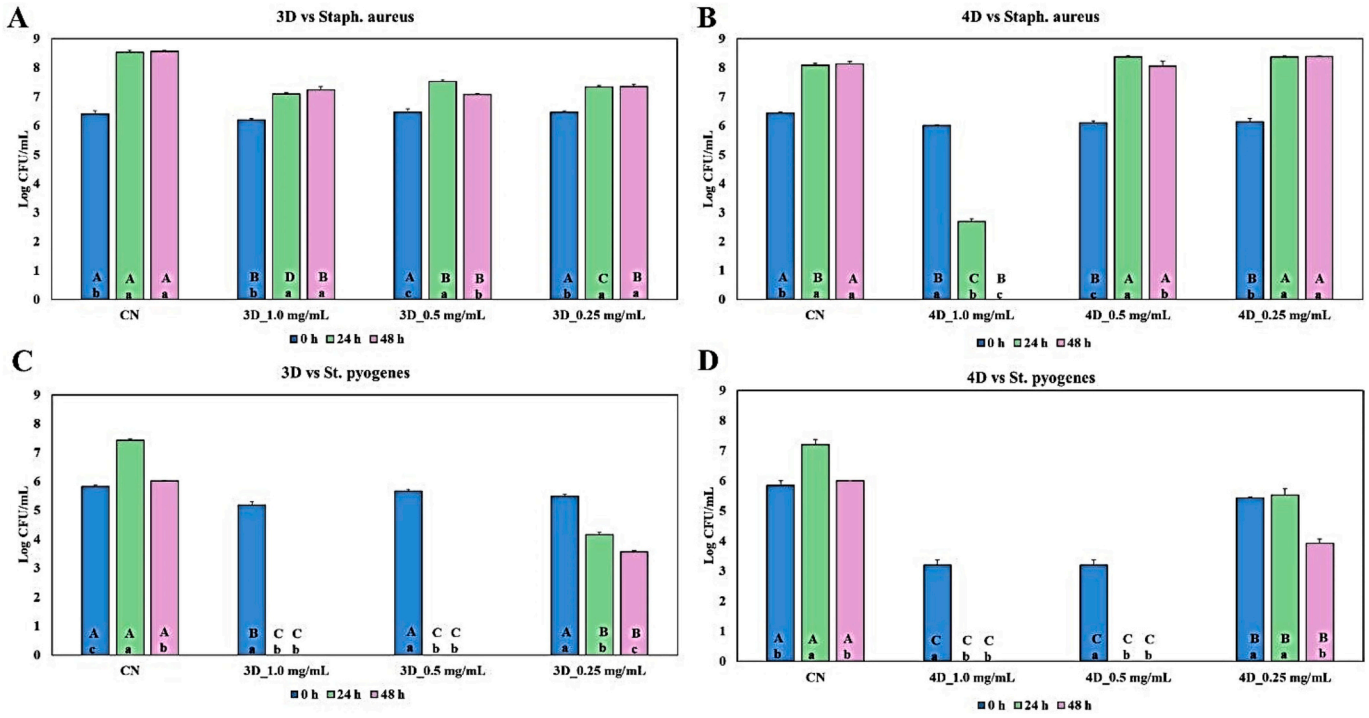

Fig. 7. Effect of different concentrations (1.0, 0.5 and 0.25 mg/mL) of 3D and 4D wax extracts on *Staph. aureus* DSM799 and *St. pyogenes* ATCC12344 over 48 h using TSB medium. Values represent the mean of independent experiments performed in triplicate ($n = 3$), and the standard deviation (SD) is indicated by bars on the histograms. Letters indicate the statistical significance of the data computed by two-way ANOVA followed by Tukey's post-hoc test ($p < 0.05$) using XLStat software (version 2012.6.02, Addinsoft Corp., Paris, France). Uppercase letters indicate statistically significant differences among different samples/treatments at the same incubation time. Lowercase letters indicate statistically significant differences within the same sample/treatment at different incubation times.

campaign, macroscopical changes were observed at the 4-day mark: the rehydration water became noticeably turbid and darker, while the broom stems exhibited significant browning and tissue softening. These physical alterations provide a mechanistic clue for the yield collapse. The darkening and turbidity are classic indicators of the oxidation of phenolic compounds and the onset of intense microbial activity (Liu et al., 2024). From a biochemical perspective, several factors likely contribute to this loss:

- Microbial Consumption: Prolonged immersion (4 days) creates an ideal environment for endogenous epiphytic microorganisms. Lipolytic bacteria and fungi can rapidly metabolize the wax fraction as a carbon source, depleting the extractable content before the Soxhlet process.
- Oxidative Polymerization: The observed browning of the biomass suggests oxidative reactions. Such processes can lead to the polymerization of unsaturated lipids, increasing their molecular weight and rendering them insoluble in non-polar solvents like n-hexane (Permadi et al., 2023).
- Matrix Entrapment: The softening of the lignocellulosic structure at 4D might facilitate the formation of stable complexes between waxes and hydrolyzed cell-wall components (like pectins), effectively trapping the lipids within a degraded matrix that n-hexane cannot penetrate (Oliveira et al., 2026).

The systematic recovery of these lipophilic markers within the core matrix strongly points toward a process-induced compositional redistribution. During the extended aqueous rehydration phase (2 to 4 days), the prolonged contact with water and subsequent tissue softening likely favored partial hydrolytic cleavage of complex cuticular wax esters. This initial hydrolysis can yield more polar amphiphilic products, such as free fatty acids and long-chain aliphatic alcohols. These liberated, lower-molecular-weight polar fragments possess enhanced mobility and altered solubility dynamics, allowing them to undergo partial redistribution and physical entrapment within the highly porous, hydrophilic lignocellulosic network of the inner core prior to Soxhlet extraction. This hypothesis is strongly supported by our parallel experimental trials, in which wax extraction directly performed on the separated outer cortex yielded only trace amounts of lipophilic compounds, confirming that the rehydration step successfully promoted a near-total depletion of the surface lipids and their subsequent redistribution into the inner residual matrix.

LC–MS/MS analysis demonstrated that wax extracts obtained under all conditions share a conserved core chemical composition dominated by long-chain fatty alcohols and wax esters forming homologous series. The repeated detection of compounds differing by 14 Da and extending to very high molecular weights ($\geq$ C56) was characteristic of linear aliphatic structures derived from very-long-chain fatty acid (VLCFA) biosynthesis in plant cuticles (Wang et al., 2020). Wax esters were identified based on diagnostic neutral losses of fatty alcohol and fatty acid moieties, consistent with fragmentation behavior reported for authentic wax esters analyzed by LC–MS/MS (Shangguan et al., 2015).

Although the qualitative composition remained largely conserved, differences in the detectability of higher-molecular-weight esters among samples suggested that extraction conditions and matrix organization influenced the effective recovery and ionization of specific wax components. Comparable chain-length distributions and ester compositions have been reported for plant-derived waxes from agricultural residues and cuticular tissues, where ester carbon numbers commonly extend beyond C40 and may reach $\geq$C56 depending on tissue type and processing (Guo et al., 2021) Hao (Hao et al., 2024). These compositional features were directly reflected in the thermal behavior observed by DSC. The progressive increase in melting temperatures and fusion enthalpies from sample 2D to samples 3D and 4D indicated a higher degree of molecular packing and crystallinity. In wax and lipid-based systems, higher melting points and enthalpy values were typically associated

with longer effective chain lengths, stronger van der Waals interactions, and more ordered crystalline domains (Tavernier et al., 2017; Freitas et al., 2018). Thermal transitions between 60 and 80 °C are commonly attributed to esterified lipids, which require higher energy for melting than free fatty acids or hydrocarbons (Zhang et al., 2011). The higher enthalpy values measured for samples 3D and 4D were therefore indicative of a larger fraction of ordered ester-rich crystalline domains, in agreement with recent reports on bio-based waxes and lipid materials (Saher et al., 2024).

SEM analysis provided direct morphological evidence supporting the DSC findings. Sample 2D exhibited a compact and weakly differentiated morphology, consistent with limited crystallinity and low fusion enthalpy. In contrast, samples 3D and 4D showed hierarchically organized crystalline networks, characterized by macrocrystalline domains decorated with dense microcrystalline features. Such multiscale organization is typical of wax and lipid systems undergoing efficient nucleation and crystal growth, where primary crystals act as templates for secondary crystallization. The increased surface roughness and interconnected crystalline framework observed for sample 4D are consistent with reports on wax-based systems displaying enhanced thermal stability and higher degrees of molecular order (Brykczynski et al., 2025a; Rinaldi et al., 2015).

Importantly, the evolution in chemical organization and solid-state structure is mirrored in the antimicrobial activity of the wax extracts.

According to the well diffusion assay, the tested wax extracts proved to be ineffective against *Gram-negative* bacteria. Likely, the outer membrane may act as an effective permeability barrier against hydrophobic compounds, such as wax constituents. Conversely, a broader spectrum of activity against Gram-positive bacteria was exhibited by 3D and 4D extracts. Such a difference might be related to the chemical composition richer in bioactive compounds. Conversely, the limited susceptibility of fungi may be related to the structural complexity of cell walls and membranes.

Wax extracts from Citrus spp. peels exhibited comparable antimicrobial activity against *Staph. aureus* (Johann et al., 2007). However, authors also reported an inhibitory effect against *E. coli*, which was not detected here, despite the similar concentration used for both studies. Antimicrobial activity against *Gram-negative* bacteria has been reported for waxes extracted from *Simmondsia chinensis* (jojoba) nuts (Alghamdi et al., 2019) and *Chaenomeles* spp. fruits (Lykholat et al., 2021), but at concentrations substantially higher than those used in the present work. Such discrepancies may arise from differences in extraction procedures, wax composition, plant cultivar, or experimental conditions.

By time–kill assay, the 3D extract exhibited bacteriostatic activity against *Staph. aureus*, whereas the 4D extract was bactericidal. However, for the *Staph. aureus* strain, the response to the wax extracts was less pronounced than that recorded for the *St. pyogenes* strain: the 4D extract induced a 3-log reduction at time zero. According to established criteria, a compound is considered bactericidal when it induces a reduction >3 log CFU/mL (99.9% kill), whereas a reduction between 0 and 3 log CFU/mL is indicative of bacteriostatic activity (Anitua et al., 2012; Shariati et al., 2020). Based on this definition, only the 4D wax extract displayed bactericidal activity against *Staph. aureus*, but only at the highest tested concentration (1.0 mg/mL).

Overall, outcomes highlight a strong species-dependent antimicrobial activity of wax extracts, with *St. pyogenes* being particularly susceptible. The prompt impact suggests that wax components may interfere with membrane integrity or essential surface-associated processes, an aspect that warrants further investigation through chemical characterization and mechanistic studies.

The integrated analysis demonstrated that antimicrobial performance was not solely dictated by wax composition but emerged from a synergistic interplay between extraction-induced accessibility, conserved aliphatic chemistry, and rehydration-dependent supramolecular organization. Moderate rehydration (3D) maximized wax recovery and structural ordering, while extended rehydration (4D) promoted further crystallinity and enhanced bactericidal activity despite lower yields. These findings underscored the importance of controlling pre-preatment conditions to tailor both the physicochemical and biological properties of bio-based waxes.

4.1. Future scope

Based on the results obtained, several research perspectives emerge to consolidate the role of Spanish broom within a sustainable, high-value biorefinery framework. A primary objective will be the optimization of the extraction process from a green chemistry perspective: the effectiveness of rehydration suggests that the use of specific enzymes (such as pectinases or cellulases) during pre-treatment could further accelerate stem delamination. This would reduce operational times and enable the replacement of n-hexane with eco-friendly solvents or supercritical fluid extraction techniques. Additionally, to fully exploit the technological.

potential of these extracts in material science, future efforts will include specific functional characterizations, such as water contact angle measurements to evaluate surface hydrophobicity and tensile testing to assess the mechanical strength of wax-derived films. Building on the selective antimicrobial efficacy observed against *Streptococcus pyogenes*, the next phase of this research will explore the integration of broom-stem waxes into specialized biomedical devices and topical formulations. The unique ability of these waxes to form organized crystalline networks makes them ideal candidates for the development of bioactive wound dressings. Future studies will focus on incorporating these crystallized wax fractions into biocompatible scaffolds to evaluate their capacity for sustained antimicrobial release and the prevention of skin-surface biofilm formation. Furthermore, the identified high-molecular-weight esters provide an excellent natural barrier. This property will be investigated for cosmeceutical applications, specifically in formulating protective ointments that restore the skin's lipid barrier while providing inherent protection against *Gram-positive* pathogens. Finally, in vitro cytocompatibility assays with human skin cells (keratinocytes and fibroblasts) will be performed to confirm the safety profile of these extracts, ensuring they meet the rigorous standards required for the pharmaceutical and personal care markets.

5. Conclusions

This study demonstrates that rehydration-assisted pre-treatment is a critical parameter for the valorization of Spanish broom stems into functional waxes. A 3-day rehydration period provided the optimal balance, yielding the highest wax recovery (~2.3% w/w) without altering the intrinsic chemical profile, which remained dominated by long-chain fatty alcohols and high-molecular-weight esters (C56).Thermal and morphological analyses revealed that longer rehydration times (3D and 4D) promoted superior molecular packing and crystallinity, directly correlating with enhanced antimicrobial activity against *Gram-positive* bacteria, particularly *Streptococcus pyogenes*. These findings indicate that simple physical pre-treatments can modulate the supramolecular organization and biological performance of broom-stem waxes, supporting their potential as sustainable, high-value ingredients for biomedical and industrial applications.

AbbreviationsThe following abbreviations are used in this manuscript:

TSB	Tryptone Soy Broth
TSA	Tryptone Soy Agar
2D	Waxes extracted from stems rehydrated for 2 days
3D	Waxes extracted from stems rehydrated for 3 days
4D	Waxes extracted from stems rehydrated for 4 days
LC-MS/MS	Liquid chromatography–tandem mass spectrometry
DSC	Differential scanning calorimetry

SEM Scanning electron microscopy

CRediT authorship contribution statement

Chiara La Torre: Methodology, Investigation, Data curation. **Antonella Buccafuri:** Investigation, Data curation. **Maria Aponte:** Investigation. **Anna di Blasio:** Investigation, Data curation. **Giuseppe Chidichimo:** Supervision, Methodology, Investigation, Data curation, Conceptualization. **Paolino Caputo:** Methodology, Investigation, Data curation. **Teresa Cerchiara:** Writing – review & editing, Visualization, Supervision. **Alessia Fazio:** Writing – review & editing, Writing – original draft, Visualization, Validation, Supervision, Data curation, Conceptualization. **Giuseppe Blaiotta:** Writing – review & editing, Writing – original draft, Validation, Supervision, Investigation, Data curation, Conceptualization.

Funding

The project work was funded by the "Ministero dell'Università e della Ricerca": Development of sustainable and innovative Spanish Broom dressings containing Glycyrrhiza glabra L. and Spanish Broom extracts to heal skin wounds (SBresswound), PRIN 2022, project n. 2022JL9S9S CUP J53D23001100006.

Declaration of competing interest

The authors declare that they have no known competing financial interests or personal relationships that could have appeared to influence the work reported in this paper.

Data availability

Data will be made available on request.

References

Alghamdi, A., Elkholy, T., Abuhelal, S., Al-Abbadi, H., Qahwaji, D., Khalifa, N., Sobhy, H., Abu Hilal, M., 2019. Antibacterial and antifungal activity of jojoba wax liquid (Simmondsia chinensis). Pharm. J. 11, 191–194.

Anitua, E., Alonso, R., Girbau, C., Aguirre Anda, J.J., Muruzabal, F., Orive, G., 2012. Antibacterial effect of plasma rich in growth factors (PRGF (R)-Endoret (R)) against Staphylococcus aureus and Staphylococcus epidermidis strains. Clin. Exp. Dermatol. 37, 652–657.

Bayés-García, L., Macridachis González, J., Calvet, T., Sato, K., 2024. In situ analyses of crystallization behavior of 1,2,3-tripalmitoyl glycerol under static and dynamic thermal conditions. J. Therm. Anal. Calorim. 149.

Benincasa, C., La Torre, C., Fazio, A., Perri, E., Caroleo, M.C., Plastina, P., Cione, E., 2021. Identification of tyrosyl oleate as a novel olive oil lipophenol with proliferative and antioxidant properties in human keratinocytes. Antioxidants 10, 1051.

Brykczynski, H., Schmidt, T., Penagos, I., Rondou, K., Van Bockstaele, F., Flöter, E., 2025a. Crystallization of wax esters in oleogels – Relevance of chain length and ester bond position. Food Struct. 44, 100429.

Brykczynski, H., Seilert, J., Flöter, E., 2025b. Prediction of melting point temperatures and enthalpies of fusion for pure wax esters using a group contribution model. Cryst. Growth Des. 25.

Bucio, A., Moreno-Tovar, R., Bucio, L., Espinosa-Dávila, J., Anguebes-Franceschi, F., 2021. Characterization of beeswax, candelilla wax and paraffin wax for coating cheeses. Coatings 11, 261.

Cheng, Y., Zhai, X., Wu, Y., Li, C., Zhang, R., Sun, C., Wang, W., Hou, H., 2022. Effects of natural wax types on the physicochemical properties of starch/gelatin edible films fabricated by extrusion blowing. Food Chem. 401, 134081.

Cherubini, F., Bird, D.N., Cowie, A., Jungmeier, G., Schlamadinger, B., Woess-Gallasch, S., 2009. Energy- and greenhouse gas-based LCA of biofuel and bioenergy systems: key issues, ranges and recommendations. Resour. Conserv. Recycl. 53, 434–447.

Chidichimo, G., Berardi, Daniela, Gullo, Giovanni, De Filpo, Giovanni, Tursi, Antonio, Basile, Maria Rita, Lania, Ilaria, De Rose, Renata, Gallo, Vincenzo, Perrotta, Aldo, 2023. Process and Plant for the Extraction of Cellulosic Fibers From Liberian Plants. Italy Patent Application IT202100005822.

Da Silva Andrade, L.B., Da Silva Julião, M.S., Carneiro Vera Cruz, R., Soares Rodrigues, T.H., Dos Santos Fontenelle, R.O., Da Silva, A.L.C., 2018. Antioxidant and antifungal activity of carnauba wax powder extracts. Ind. Crop. Prod. 125, 220–227.

Doan, C.D., Ta, C.M., De Vrieze, M., Lynen, F., Danthine, S., Brown, A., Dewettinck, K., Patel, A.R., 2017. Chemical profiling of the major components in natural waxes to elucidate their role in liquid oil structuring. Food Chem. 214, 717–725.

Freitas, G.B., Duncke, A.C., Barbato, C.N., De Oliveira, M.C.K., Pinto, J.C., Nele, M., 2018. Influence of wax chemical structure on W/O emulsion rheology and stability. Colloids Surf. A Physicochem. Eng. Asp. 558, 45–56.

Gimeno, T., Camarero, J., Granda, E., Pías, B., Valladares, F., 2012. Enhanced growth of Juniperus thurifera under a warmer climate is explained by a positive carbon gain under cold and drought. Tree Physiol. 32, 326–336.

Gundupalli, M., Chuetor, S., Cheenkachorn, K., Rattanaporn, K., Show, P.-L., Cheng, Y.-S., Sriariyanun, M., 2021. Interferences of waxes on enzymatic saccharification and ethanol production from lignocellulose biomass. Bioengineering 8, 171.

Guo, X., Pethica, B., Huang, J., Prud'homme, R., 2005. Effect of cooling rate on crystallization of model waxy oils with microcrystalline poly(ethylene butene). Energy Fuels 20.

Guo, J., Huang, K., Rou, C., Zhang, J., Xu, Y., 2021. Aliphatic extractive effects on acetic acid catalysis of typical agricultural residues to xylo-oligosaccharide and enzymatic hydrolyzability of cellulose. Biotechnol. Biofuels 14.

Hao, X., Lv, J., Zhao, Z., Tong, Y., Deng, M., Wen, J., 2024. Compositional variances in petal cuticular wax of eight rose species and their impacts on vase life under water-loss stress. Front. Plant Sci. 15.

Irimia, C., Yumusak, C., Schimanofsky, C., Kanbur, Y., Ban, B., Ciganek, M., Sedlacek, P., Krajčovič, J., D'orsi, R., Operamolla, A., Salinas, Y., Brüggemann, O., Petritz, A., Stadlober, B., Mourya, R., Teichert, C., Langhals, H., Sariciftci, N., Irimia-Vladu, M., 2025. Natural waxes from plant and animal origin as dielectrics for low-voltage organic field effect transistors. J. Mater. Chem. C 13.

Johann, S., Oliveira, V., Pizzolatti, M., Schripsema, J., Braz-Filho, R., Branco, A., Jr, A., 2007. Antimicrobial activity of wax and hexane extracts from Citrus spp. peels. Mem. Inst. Oswaldo Cruz 102.

Kończak, B., Uszok, E., Białowąs, M., Wiesner-Sękala, M., Zawartka, P., Klus, M., Klus, L., 2026. Biodegradation of hydrophobic coatings based on natural wax and its mixtures, 18, 509.

La Torre, C., Caputo, P., Plastina, P., Cione, E., Fazio, A., 2021. Green husk of walnuts (*Juglans regia* L.) from Southern Italy as a valuable source for the recovery of glucans and pectins. Fermentation 7, 305.

La Torre, C., Plastina, P., Abrego-Guandique, D.M., Caputo, P., Oliviero Rossi, C., Saraceno, G.F., Caroleo, M.C., Cione, E., Fazio, A., 2024. Characterization of exopolysaccharides isolated from donkey milk and its biological safety for skincare applications. Polysaccharides 5, 493–503.

Lísa, M., Holčapek, M., 2015. High-throughput and comprehensive lipidomic analysis using ultrahigh-performance supercritical fluid chromatography–mass spectrometry. Anal. Chem. 87, 7187–7195.

Liu, C., Fan, H., Zhang, J., Wu, J., Zhou, M., Cao, F., Tao, G., Zhou, X., 2024. Combating browning: mechanisms and management strategies in in vitro culture of economic woody plants. For. Res. 4.

Luo, W., Gonzalez, E., Zarei, A., Calleja, S., Rozzi, B., Demieville, J., Li, H., Truco, M.-J., Lavelle, D., Michelmore, R., Dyer, J.M., Jenks, M.A., Pauli, D., 2024. Leaf cuticular wax composition of a genetically diverse collection of lettuce (Lactuca sativa L.) cultivars evaluated under field conditions. Heliyon 10, e27226.

Lykholat, Y., Khromykh, N., Didur, O., Sklyar, T., Holubieva, T., Lykholat, T., Lavrentieva, K., Liashenko, O., 2021. GC-MS analysis of cuticular waxes and evaluation of antioxidant and antimicrobial activity of Chaenomeles cathayensis and Ch. × californica fruits. Regul. Mech. Biosyst. 12, 718–723.

Malyzhenkov, P., Chidichimo, G., La Torre, C., Fazio, A., 2025. Spanish broom production chain improvement with a view to sustainable development, 13, 54.

Nghiem, N., O'connor, J., Hums, M., 2018. Integrated process for extraction of wax as a value-added co-product and improved ethanol production by converting both starch and cellulosic components in Sorghum grains. Fermentation 4.

Ntunka, M., Makhathini, T., Khuamlo, S., Bwapwa, J., Tshibangu, M., 2025. Recent developments in the valorization of sugarcane bagasse biomass via integrated pretreatment and fermentation strategies. Fermentation 11, 632.

Oliveira, B., Nascimento, V., Polizeli, M.D.L., 2026. *Burkholderia lata* BL02 Galactolipase as an Important Biocatalyst for Plant Biomass Deconstruction and Sugar Ester Synthesis.

Padar, S., Jeelani, S., Windhab, E., 2008. Crystallization kinetics of cocoa fat systems: experiments and modeling. J. Oil Fat Ind. 85, 1115–1126.

Pashova, S., 2023. Application of plant waxes in edible coatings. Coatings 13, 911.

Permadi, N., Nurzaman, M., Alhasnawi, A., Doni, F., Julaeha, E., 2023. Managing lethal browning and microbial contamination in Musa spp. tissue culture: synthesis and perspectives. Horticulturae 9, 453.

Pipintakos, G., Soenen, H., Goderis, B., Blom, J., Lu, X., 2022. Crystallinity of bitumen via WAXD and DSC and its effect on the surface microstructure. Crystals 12.

Principato, L., Carullo, D., Bassani, A., Gruppi, A., Duserm Garrido, G., Dordoni, R., Spigno, G., 2021. Effect of dietary fiber and thermal conditions on rice bran wax-based structured edible oils. Foods 10.

Qi, G., Peng, F., Xiong, L., Lin, X., Huang, C., Li, H., Chen, X., Chen, X., 2017. Extraction and characterization of wax from sugarcane bagasse and the enzymatic hydrolysis of dewaxed sugarcane bagasse. Prep. Biochem. Biotechnol. 47, 276–281.

Rahman, T., Shao, M., Pahari, S., Venglat, P., Soolanayakanahally, R., Qiu, X., Rahman, A., Tanino, K., 2021. Dissecting the roles of cuticular wax in plant resistance to shoot dehydration and low-temperature stress in Arabidopsis. Int. J. Mol. Sci. 22, 1554.

Regert, M., 2009. Direct Mass Spectrometry to Characterise Wax and Lipid Materials.

Righetti, M.C., 2017. Crystallization of polymers investigated by temperature-modulated DSC. Materials 10, 442.

Rinaldi, M., Paciulli, M., Dall'asta, C., Cirlini, M., Chiavaro, E., 2015. Short-term storage evaluation of quality and antioxidant capacity in chestnut-wheat bread. J. Sci. Food Agric. 95.
Rodionova, M., Bozieva, A., Zharmukhamedov, S., Yoong Kit, L., Lan, J., Veziroglu, A., Veziroglu, T., Tomo, T., Chang, J.-S., Allakhverdiev, S., 2021. A comprehensive review on lignocellulosic biomass biorefinery for sustainable biofuel production. Int. J. Hydrog. Energy 47.
Rossello, S., Mandrone, M., Cerchiara, T., Chiocchio, I., Rossi, M., Chinnici, F., Sallustio, V., Aponte, M., Blaiotta, G., Luppi, B., Angela, A., Bigucci, F., Cappadone, C., 2024. A new wound-healing tool based on Glycyrrhiza glabra extract-loaded ufasomes on Spanish broom dressings. Molecules 29, 3811.
Ruguo, Z., Hua, Z., Hong, Z., Ying, F., Kun, L., Wenwen, Z., 2011. Thermal analysis of four insect waxes based on differential scanning calorimetry (DSC). Procedia Eng. 18, 101–106.
Saher, S., Piper, S., Forsyth, C., Kar, M., Macfarlane, D., Pringle, J., Matuszek, K., 2024. Investigation of the intermolecular origins of high and low heats of fusion in azolium salt phase change materials for thermal energy storage. Mater. Adv. 5.
Sasounian, R., Martinez, R., Lopes, A., Giarolla, J., Rosado, C., Magalhães, W., Velasco, M., Baby, A., 2024. Innovative approaches to an eco-friendly cosmetic industry: a review of sustainable ingredients. Clean Technol. 6, 176–198.
Shangguan, L., Zhang, L., Xiong, Z., Ren, J., Zhang, R., Gao, F., Zhang, W., 2015. Investigation of bi-enzymatic reactor based on hybrid monolith with nanoparticles embedded and its proteolytic characteristics. J. Chromatogr. A 1388, 158–166.
Shariati, A., Dadashi, M., Moghadam, M.T., Van Belkum, A., Yaslianifard, S., Darban-Sarokhalil, D., 2020. Global prevalence and distribution of vancomycin resistant, vancomycin intermediate and heterogeneously vancomycin intermediate Staphylococcus aureus clinical isolates: a systematic review and meta-analysis. Sci. Rep. 10, 12689.
Silva, G., Henriques, J., Martinez, P., 2022. Sugarcane wax extraction using hexane and limonene mixtures. Revista Engenhariana Agricultura 30, 13–18.
Simões, R., Miranda, I., Pereira, H., 2022. The influence of solvent and extraction time on yield and chemical selectivity of cuticular waxes from Quercus suber leaves. Processes 10, 2270.
Singh, D., Sengar, M., Gupta, T., Singh, S., Singh, D., Mishra, V., Dev, R., Giri, B.S., 2024. Natural wax recovery from Musa acuminata biomass using organic solvents. Chemosphere 363, 142919.
Tavernier, I., Doan, C., Walle, D., Danthine, S., Rimaux, T., Dewettinck, K., 2017. Sequential crystallization of high and low melting waxes to improve oil structuring in wax-based oleogels. RSC Adv. 7, 12113–12125.
Tunstad, S.A., Bull, I.D., Rands, S.A., Whitney, H.M., 2024. The cuticular wax composition and crystal coverage of leaves and petals differ in a consistent manner between plant species. Open Biol. 14, 230430.
Vrkoslav, V., Urbanová, K., Háková, M., Cvačka, J., 2013. Analysis of wax esters by silver-ion high-performance liquid chromatography-tandem mass spectrometry. J. Chromatogr. A 1302.
Wang, X., Kong, L., Zhi, P., Chang, C., 2020. Update on Cuticular Wax Biosynthesis and Its Roles in Plant Disease Resistance, 21, 5514.
Xue, D., Zhang, X., Lu, X., Guang, C., Chen, Z.-H., 2017. Molecular and evolutionary mechanisms of cuticular wax for plant drought tolerance. Front. Plant Sci. 08, 621.
Zhang, R., Zhang, H., Zhang, Z., Zheng, H., Feng, Y., Zhang, W., 2011. Characterization of five natural resins and waxes by differential scanning calorimetry (DSC). Adv. Mater. Res. 418-420, 643–650.